Available online at www.sciencedirect.com
ScienceDirect
Journal of Sound and Vibration 301 (2007) 93–105
JOURNAL OF SOUND AND VIBRATION
www.elsevier.com/locate/jsvi

Structural-acoustic optimization of sandwich structures with cellular cores for minimum sound radiation

H. Denli, J.Q. Sun*

Department of Mechanical Engineering, University of Delaware, Newark, DE 19716, USA

Received 8 February 2006; received in revised form 31 May 2006; accepted 11 September 2006
Available online 14 November 2006

Abstract

An optimization study of sandwich structures with cellular cores for minimum noise radiation in a wide frequency band, subject to the constraints on the fundamental frequency and weight is presented. Sensitivity functions of the radiated acoustic power are used to improve the computational time and accuracy in near optimization. Numerical examples indicate that significant reduction of narrowband and broadband sound radiation can be achieved.

1. Introduction

Since sandwich structures in aerospace industry are often stiff and light, and have low damping, they can experience resonant motions and radiate sound. Advanced sandwiches structures must meet not only stiffness to weight ratio demands, but also have improved acoustic performance. An optimization study of the cellular core of sandwich structures to minimize the radiated sound power in a wide frequency band, subject to the constraints on the fundamental frequency and weight is presented.

Sandwich structures consist of three layers. Two thin and stiff skins are bonded to a low density core on both sides. The skins usually carry the in-plane loads and bending moments, while the core, which has lower stiffness compared to the skins, resists the transverse shear loads. The advantage of composite sandwich structures lies in that they possess large bending or torsional rigidity with very low-specific weights; they also provide an excellent platform for optimization of structures to meet various objectives. Minimum weight sandwiches have been studied extensively [1,2]. Optimization of sandwich structure for sound reduction is more challenging, and has been studied by a few researchers [3–5]. The present study is focused on sandwich structures with a cellular, frame-like core.

The multifunctional properties of cellular solids have generated a great deal of interest for their application in the aerospace industry. The topological design of periodic multifunctional core structures has been explored, and the relationship between topology and performance has been established by Evans, Hutchinson, Fleck, Ashby and Wadley [6]. Vibration of sandwich beams with a honeycomb truss core is analyzed in Ref. [7]. A unit cell analysis to investigate the effect of its resonance is also presented in this reference. It has

*Corresponding author. Tel.: +1 302 831 8686; fax: +1 302 831 3619.
E-mail address: jqsun@udel.edu (J.Q. Sun).

0022-460X/$ - see front matter © 2006 Elsevier Ltd. All rights reserved.
doi:10.1016/j.jsv.2006.09.025

been found out that the individual cell may be used as a design tool to attenuate the vibration. The acoustic behavior of negative Poisson ratio cellular structures has been studied in the literature [8,9]. Other studies have demonstrated that the structural-acoustic optimization may not result in any overall structural pattern (periodicity) when the band of frequencies being studied includes more than one mode of the structure. This can be caused by the complex interactions among the modes in and near the band [10,11].

The structural-acoustic optimization studies can be done in two ways. The first approach computes the radiated acoustic power from the structural motion directly and then minimizes the acoustic power [4]. The second approach proposes first to develop surface velocity profiles for the structure with minimum acoustic radiation known as "weak radiators" [12], and then optimizes the structure to meet the desired velocity profiles [13]. The present work follows the first approach.

This paper is focused on shape optimization of hexagonal truss core sandwich beams. The parameters affecting the shape of the unit cell are considered as design parameters. The total weight and fundamental frequency are constrained. We first analyze the sound radiation from the sandwiches with two periodic cores: honeycomb and re-entrant, and then examine the sensitivity of the acoustic power with respect to shape changes of the unit cells in these cores.

The paper is organized as follows. Firstly, we present the geometry of the cellular core and model the equations of motion of the structure by finite elements. Secondly, we obtain the acoustic power radiated by the structure by using the Rayleigh integral leading to a quadratic form in terms of the normal velocities on the radiating surface of the sandwich. Thirdly, we study the variation of the radiated acoustic power with respect to the shape change of unit cells. Fourthly, we formulate the sensitivity of the radiated acoustic power, resonant frequencies and weight of the sandwich with respect to design variables. Finally, we study the optimization problem for minimizing the radiated acoustic power with respect to a set of design parameters which control the shape of the individual unit cell. The constraints on the fundamental frequency and weight are imposed in the optimization. The optimization problem is solved by using a quasi-Newton method. Numerical results are presented to demonstrate the theoretical development.

2. Theoretical formulation

2.1. Configuration

Rectangular, honeycomb and re-entrant types of core structures are widely studied in prismatic core sandwiches [14]. Other periodic topologies such as chiral comb also exist for the core [15]. Here, we consider sandwich beams with a cellular truss-core as shown in Fig. 1 where the skins and cores are separated for illustration. The upper part of the figure depicts the honeycomb beam. The lower one shows the re-entrant core beam. Note that the re-entrant core has a negative Poisson ratio. Although we consider periodic cell topology in the analysis part of the study, later we shall allow generations of aperiodic cell topologies via design parameters and let the optimization process shape them.

The sandwich structure is exposed to a plane wave of acoustic pressure at the top surface as shown in Fig. 2 and radiates to the semi-infinite space. We assume that the sandwich beam is infinitely baffled at the upper and lower surfaces. Fig. 2 also displays the observation surface where the acoustic power radiated from the beam is computed.

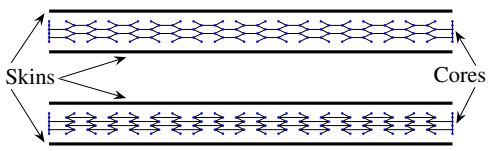

Fig. 1. Beams with hexagonal cores. The top core consists of honeycomb cells and the bottom core consists of re-entrant cells. The skins and cores are separated for illustration purpose.

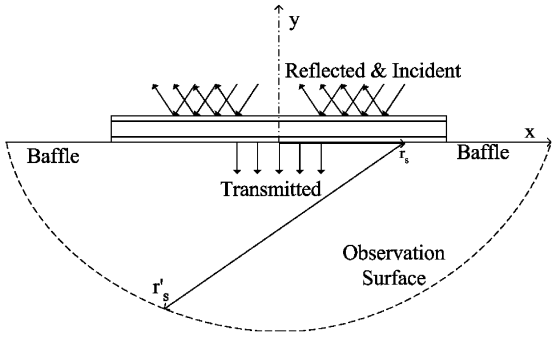

Fig. 2. Structural and acoustical coordinate systems.

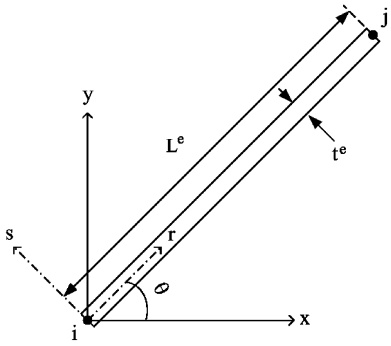

Fig. 3. Local and global coordinate systems of a frame element.

2.2. Finite element modeling of the sandwich beam

The core of the sandwich consists of two dimensional frames modeled as Euler–Bernoulli beams. In Fig. 3 two coordinate systems: a local coordinate system (r, s) and a global coordinate system (x, y) are shown. We shall derive equations of motion by applying Hamilton's principle

$$\int_{t_1}^{t_2} \delta(T - U + W)\,\mathrm{d}t = 0, \tag{1}$$

where T and U are the kinetic and strain energies of the system, and δW is the virtual work done by the external forces. The strain and kinetic energies of all the elements in the local coordinate system are given in the same form as

$$U^{(e)} = \frac{1}{2}EA\int_0^{L^e} u_r^2(r,t)\,\mathrm{d}r + \frac{1}{2}EI\int_0^{L^e} w_{rr}^2(r,t)\,\mathrm{d}r,$$

$$T^{(e)} = \frac{1}{2}\rho A\int_0^{L^e} u_t^2(r,t)\,\mathrm{d}r + \frac{1}{2}\rho A\int_0^{L^e} w_t^2(r,t)\,\mathrm{d}r, \tag{2}$$

where E and ρ are Young's modulus and the mass density of the element, A and I are, respectively, the cross-sectional area and the second-order moment of the beam element cross section. Subscripts r and t denote partial derivatives with respect to the local coordinate and time, respectively.

The virtual work done by the external forces on an element can be expressed as

$$\delta W^{(e)} = \int_0^{L^e} \delta u(r,t) f_u(r,t)\,\mathrm{d}r + \int_0^{L^e} \delta w(r,t) f_w(r,t)\,\mathrm{d}r, \tag{3}$$

where $f_u(r,t)$ and $f_w(r,t)$ are longitudinal and transverse excitations per unit length acting on the element. In the following, we shall consider harmonic vibrations only. We assume the element solution to be in the form

$$u(r,\omega) = \mathbf{N}_u(r)\cdot\mathbf{u}^{(e)}(\omega),$$

$$w(r,\omega) = \mathbf{N}_w(r)\cdot\mathbf{w}^{(e)}(\omega), \tag{4}$$

where $\mathbf{N}_u(r)$ and $\mathbf{N}_w(r)$ are the Hermitian shape function for longitudinal and transverse displacements, and $\mathbf{u}^{(e)}(\omega) = [u_i u_j]^{\mathrm{T}}$ and $\mathbf{w}^{(e)}(\omega) = [w_i, \theta_i, w_j, \theta_j]^{\mathrm{T}}$ where i, j are node numbers and $\theta = \partial w/\partial r$. Hamilton's principle leads to the equations of motion in terms of the global nodal displacement vector $\tilde{\mathbf{u}}$

$$(\hat{\imath}\beta - \omega^2)\mathbf{M}\tilde{\mathbf{u}}(\omega) + (1 + \hat{\imath}\alpha)\mathbf{K}\tilde{\mathbf{u}}(\omega) = \mathbf{f}(\omega), \quad \hat{\imath} = \sqrt{-1}, \tag{5}$$

where $\tilde{\mathbf{u}}$ is the assembled generalized displacement vector combined from the local vectors $\mathbf{u}^{(e)}$ and $\mathbf{w}^{(e)}$, $\mathbf{M}$, $\mathbf{K}$ and $\mathbf{f}(\omega)$ are the assembled element mass and stiffness matrices and nodal forces. They are also assembled from their directional correspondents given in the following form:

$$\mathbf{M}_u = \int_0^{L^e} \mathbf{N}_u^{\mathrm{T}} \rho A \mathbf{N}_u\,\mathrm{d}r, \quad \mathbf{K}_u = \int_0^{L^e} \left(\frac{\mathrm{d}\mathbf{N}_u}{\mathrm{d}r}\right)^{\mathrm{T}} EA \frac{\mathrm{d}\mathbf{N}_u}{\mathrm{d}r}\,\mathrm{d}r,$$

$$\mathbf{M}_w = \int_0^{L^e} \mathbf{N}_w^{\mathrm{T}} \rho A \mathbf{N}_w\,\mathrm{d}r, \quad \mathbf{K}_u = \int_0^{L^e} \left(\frac{\mathrm{d}^2\mathbf{N}_w}{\mathrm{d}r^2}\right)^{\mathrm{T}} EI \frac{\mathrm{d}^2\mathbf{N}_w}{\mathrm{d}r^2}\,\mathrm{d}r,$$

$$\mathbf{f}_u^{(e)} = \int_0^{L^e} \mathbf{N}_u^{\mathrm{T}} f_u\,\mathrm{d}r, \quad \mathbf{f}_w^{(e)} = \int_0^{L^e} \mathbf{N}_w^{\mathrm{T}} f_w\,\mathrm{d}r. \tag{6}$$

In the derivation, we have also assumed a Rayleigh damping matrix $\mathbf{C} = \alpha\mathbf{K} + \beta\mathbf{M}$ where α and β are prespecified constants.

3. Acoustic radiation

Assume that a plane acoustic wave of frequency ω is incident upon the upper surface of the beam where $x = r$, the resultant pressure amplitude of incident and reflected pressures at the top surface of the beam is $p = 2A$, where A is the incident pressure amplitude. Thus, the nodal force vector at the top of the surface can be calculated as

$$\mathbf{f}_w^{(e)} = 2A \int_0^{L^e} \mathbf{N}_w^{\mathrm{T}}(x)\,\mathrm{d}x. \tag{7}$$

On the bottom surface of the beam shown in Fig. 2, the transmitted acoustic pressure $p_t(\mathbf{r}_{S'})\mathrm{e}^{\hat{\imath}\omega t}$ at an observation point $\mathbf{r}_{S'}$ due to the surface normal velocity $v(\mathbf{r}_S)$ of the beam can be obtained by using the Rayleigh integral as

$$p_t(\mathbf{r}_{S'}) = \frac{\hat{\imath}\omega\rho_a}{2\pi} \int_S v(\mathbf{r}_S) \frac{\mathrm{e}^{-\hat{\imath}kR}}{R}\,\mathrm{d}S, \tag{8}$$

where ρ_a is the air density, $\mathbf{r}_S$ is the position vector of the surface element $\mathrm{d}S$ with the normal velocity $v(\mathbf{r}_S)$, S is the vibrating surface of the beam, and $R = |\mathbf{r}_S - \mathbf{r}_{S'}|$. The acoustic power W radiated from the baffled beam is given by an integration over the receiver surface S'

$$W(\omega) = \frac{1}{2}\int_{S'}\int_S v(\mathbf{r}_S)\left(\frac{\omega\rho_a}{2\pi}\frac{\sin(kR)}{R}\right) v^*(\mathbf{r}_{S'})\,\mathrm{d}S\,\mathrm{d}S', \tag{9}$$

where the asterisk indicates complex conjugate.

To compute the radiated power in finite elements, we take linear shape functions to approximate the velocity distribution over an element, and use Gaussian quadrature to compute the integration. The effort for the acoustic power calculation is proportional to the fourth power of the order of the integration. Here, we use a single-point integration scheme to reduce the computational effort. The difference of the power computed when using the single point and higher point integrations is about 1% when the element size is at least few times smaller than the shortest acoustic wavelength in the band [16].

Let the velocity of the kth element be in the form

$$v_k(r,s) = \mathbf{H}(r,s)\mathbf{v}^{(k)}, \tag{10}$$

where $\mathbf{H}(r,s)$ is a vector of shape functions, and $\mathbf{v}^{(k)}$ is the nodal normal velocity vector of the element. We express the radiated acoustic power W as

$$W(\omega) = \frac{1}{2}\sum_{m=1}^{M}\sum_{n=1}^{N}\mathbf{v}^{(m)\mathrm{T}}\mathbf{B}_{mn}\mathbf{v}^{*(n)}, \tag{11}$$

where M and N are the number of elements in the receiver and source surfaces

$$\mathbf{B}_{mn} = g_1\frac{\omega\rho_a}{2\pi}J_mJ_n\frac{\sin(kR_{mn})}{R_{mn}}\mathbf{H}^{\mathrm{T}}\mathbf{H}\Big|_{\substack{r=\bar{r}\\ s=\bar{s}}} \tag{12}$$

and $\bar{r}$ and $\bar{s}$ are the integration points on the receiver and source elements, respectively, J_m and J_n are the Jacobians at the integration points, and g_1 is the Gaussian weighting coefficient for the single-point integration. Eq. (12) can be readily extended to the case where multiple Gaussian integration points are used.

After the assembly, the radiated acoustic power is

$$W(\omega) = \tfrac{1}{2}\mathbf{v}^{\mathrm{T}}\mathbf{B}\mathbf{v}^{*}. \tag{13}$$

Note that $\mathbf{B}$ is Hermitian such that $\mathbf{B} = \mathbf{B}^{H}$. The acoustic power radiated from the structure is a function of frequency. In this work, the excitation frequency varies over a band which may include resonant frequencies of the structure. The objective is to minimize the radiated power over this band. The frequency averaged sound power over the band can be obtained by integrating W over the frequency band:

$$W_a = \frac{1}{\omega_2-\omega_1}\int_{\omega_1}^{\omega_2}W(\omega)\,\mathrm{d}\omega \simeq \frac{1}{\omega_2-\omega_1}\sum_{i=1}^{m}W(\omega_i)\Delta\omega_i. \tag{14}$$

3.1. Analysis of the radiated acoustic power

Acoustic radiation from honeycomb and re-entrant core beams are compared in this section. We consider a uniform beam 2 m long made out of 10 cm thick core and 1 cm thick upper and lower skins. The core of the beam is discretized with 20 nodes in longitudinal direction and 6 nodes in the thickness direction. This discretization scheme generates 19 cells in the longitudinal direction and $2\frac{1}{2}$ cells in the thickness direction as shown in Fig. 1. Every cell edge thickness is 1 cm thick. Both upper and lower skins and core are made of the same material. Its modulus of elasticity is 0.71×10^{11} Pa and its density is $2700\,\mathrm{kg/m^3}$. The boundary conditions are assumed to be simply supported at both ends where the upper and lower faces are connected to rigid baffles.

In Fig. 4 the variation of radiated sound power in frequency ranging from 25 to 1500 Hz is shown. As seen from the figure, the re-entrant core transmits less sound than honeycomb core. The frequency averaged power difference between re-entrant and honeycomb sandwich beam from 25 to 1500 Hz is 3.43 dB and from 100 to 1000 Hz is 5.36 dB. On the other hand, the fundamental frequency of the re-entrant beam is at 51.90 Hz while the honeycomb one's is at 102.25 Hz. Besides, the total area covered by re-entrant core is $0.097\,\mathrm{m^2}$ and the area by honeycomb is $0.068\,\mathrm{m^2}$. Note that the bending stiffness to weight ratio of the sandwich is related to the fundamental frequency. The re-entrant sandwich beam possesses about 1/3 times the lower bending stiffness

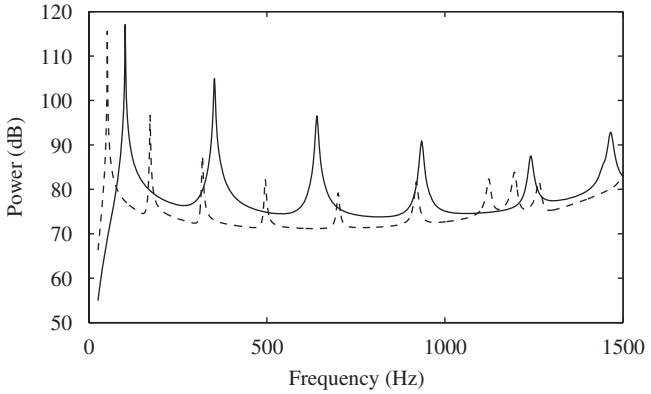

Fig. 4. Spectral distribution of the radiated sound power of the optimized and baseline beams. Solid and dashed lines refer to honeycomb and re-entrant core beams, respectively.

to weight ratio than the honeycomb beam. These results motivate us to find the optimum core topology which radiates the minimum sound power while satisfying weight and fundamental frequency constraints.

4. Sensitivity analysis

Sensitivity plays an important role in optimization studies. In particular, analytical expressions of sensitivity can improve computational efficiency and accuracy at the same time [17]. One rigorous technique to formulate sensitivity of structural acoustic problems is known as the adjoint variable method [18,19]. Here, we derive as many explicit expressions for sensitivities as possible. The other sensitivity calculations are computed by the finite difference method during the optimization. It should be noted that the eigenvalue problem takes the majority of computational effort in the optimization procedure. Therefore, the sensitivity functions of power and natural frequencies with respect to design parameters are derived by the differentiation of the equations of motion.

4.1. Sensitivity of acoustic power

Assume that the sound power is a function of a set of design variables denoted by b_k. Differentiating Eq. (14) with respect to b_k, we obtain

$$\frac{\partial W_a}{\partial b_k} = \frac{1}{\omega_2 - \omega_1} \sum_{i=1}^{m} \left(\mathbf{v}^{\mathrm{T}} \mathbf{B} \frac{\partial \mathbf{v}^*}{\partial b_k} + \frac{1}{2} \mathbf{v}^{\mathrm{T}} \frac{\partial \mathbf{B}}{\partial b_k} \mathbf{v}^* \right)_{\omega_i} \Delta\omega_i. \tag{15}$$

The Hermitian coupling matrix $\mathbf{B}$ is in general a function of frequency and the geometry of the radiating surface of the structure. In this study, we assume that the excitation frequency and the geometry of the radiating surface are not altered by the design parameters so that $\partial \mathbf{B}/\partial b_k = 0$.

Differentiating Eq. (5) with respect to b_k, we obtain

$$[(\hat{\imath}\beta - \omega^2)\mathbf{M} + (1 + \hat{\imath}\alpha)\mathbf{K}] \frac{\partial \tilde{\mathbf{u}}}{\partial b_k} = -\left[(\hat{\imath}\beta - \omega^2) \frac{\partial \mathbf{M}}{\partial b_k} + (1 + \hat{\imath}\alpha) \frac{\partial \mathbf{K}}{\partial b_k} \right] \tilde{\mathbf{u}}, \tag{16}$$

where we have assumed that $\partial \mathbf{f}/\partial b_k = \mathbf{0}$. Note that $\partial \tilde{\mathbf{u}}/\partial b_k$ can be obtained from Eq. (16) where $\partial \mathbf{M}/\partial b_k$, $\partial \mathbf{K}/\partial b_k$ and $\tilde{\mathbf{u}}$ are available. In the numerical examples reported below, derivatives of mass and stiffness matrices are computed by using the finite difference method to decrease the level of implementation complexity. Sensitivity of the harmonic velocity response is given by

$$\frac{\partial \mathbf{v}}{\partial b_k} = \hat{\imath}\bar{\omega} \frac{\partial \tilde{\mathbf{u}}}{\partial b_k}. \tag{17}$$

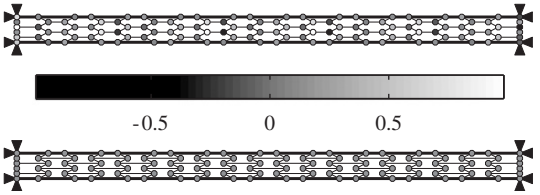

Fig. 5. The sensitivity of the frequency averaged power W_a with respect to the longitudinal displacement of the nodes. The top plot is for a honeycomb beam and the bottom one is for a re-entrant beam. Each circle shading level depicts the relative sensitivity which is normalized by its maximum amplitude.

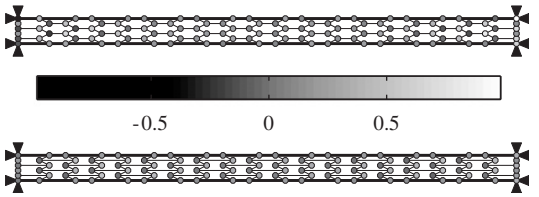

Fig. 6. The sensitivity of the fundamental frequency with respect to the longitudinal displacement of the nodes. The top plot is for a honeycomb beam and the bottom one is for a re-entrant beam. Each circle shading level depicts the relative sensitivity which is normalized by its maximum amplitude.

As an example, the sensitivity of the radiated sound power with respect to the longitudinal displacement of the core nodes is computed for honeycomb and re-entrant sandwich beams as shown in Fig. 5. We consider the same topologies as introduced in Section 3.1. The frequency band is chosen to be from 100 to 1000 Hz to compute the frequency averaged sensitivity of the beams. It is seen from Fig. 5 that the radiated acoustic power from honeycomb sandwich beam is more sensitive to node displacements than the re-entrant one. It is obvious from the sensitivity resolution of honeycomb beam that movements of the interior nodes affect the radiated sound power more than the face nodes which are connected to skins. This is because the interior nodes influence the shape change of the core more than the face nodes. Moreover, the honeycomb sensitivity plot shows that the sensitivity distribution among the nodes appears to be antisymmetric along the length of the beam, although this anti-symmetry may not exist in other frequency bands.

4.2. Sensitivity of natural frequencies

Since the fundamental frequency of the structure is used as a constraint, its sensitivity with respect to the design parameters can be obtained by differentiating the following eigenvalue problem:

$$[\mathbf{K} - \lambda_j \mathbf{M}]\phi_j = 0 \text{ and } \phi_j^{\mathrm{T}} \mathbf{M} \phi_j = \mathbf{I}. \tag{18}$$

We have

$$\lambda_{j,k} = \phi_j^{\mathrm{T}} \left[\frac{\partial \mathbf{K}}{\partial b_k} - \lambda_i \frac{\partial \mathbf{M}}{\partial b_k} \right] \phi_j. \tag{19}$$

Note that λ_1 denotes the fundamental frequency.

In Fig. 6, the sensitivity of the fundamental frequency with respect to the node movements of the honeycomb and re-entrant sandwich beams is shown. Sensitivity levels of the beams with honeycomb and re-entrant cores are about the same except for the left and right end nodes. Anti-symmetry of sensitivity distribution along the length of the beam remains. These analyses of sensitivities with respect to the design parameters also reinforce that there must exist a compromising solution that minimizes the acoustic radiation while fulfilling the fundamental frequency constraint.

5. Structural optimization

The structural-acoustic optimization problem is stated as

$$\text{minimize} \quad W_a(\mathbf{b}) = \frac{1}{\omega_2 - \omega_1} \int_{\omega_1}^{\omega_2} W(\omega, \mathbf{b})\, \mathrm{d}\omega, \tag{20}$$

$$\text{subject to} \quad \left\{ \begin{array}{c} b_i^l \leqslant b_i \leqslant b_i^u \\ \sum_{i=1}^{n} m_i - m_0 \leqslant 0 \\ -\omega_f(\mathbf{b}) + \omega_0 \leqslant 0 \end{array} \right\}, \tag{21}$$

where b_i^l and b_i^u are the lower and upper bounds of the ith design parameter, m_i is the mass of the ith frame element, m_0 is the allowable maximum total mass, $\omega_f(\mathbf{b})$ is the fundamental frequency of the beam and ω_0 is the allowable minimum fundamental frequency. The lower and upper bounds of the design parameters are set to avoid excessive element distortion and inconsistent cell geometry. An optimal solution is a structure that radiates minimum acoustic power in the given frequency band and satisfies the set of constraints.

Assume that there are m inequality constraints and n equality constraints. The inequality constraints can be converted to equality constraints by introducing m slack variables as follows:

$$c_j(b_1, \ldots, b_n) + b_{j+n}^2 = 0, \quad j = 1, \ldots, m, \tag{22}$$

where $c_j(b_1, \ldots, b_n)$ is shorthand notation for the constraint function. We expand the design parameter vector to be $\mathbf{b} = [b_1, \ldots, b_n, \ldots, b_{n+m}]^{\mathrm{T}}$. Define the Lagrangian function

$$L(\mathbf{b}, \boldsymbol{\lambda}) = W_t(\mathbf{b}) + \boldsymbol{\lambda}^{\mathrm{T}} \mathbf{c}(\mathbf{b}), \tag{23}$$

where $\boldsymbol{\lambda} \in R^{n+m}$ denotes a set of Lagrange multipliers. The quasi-Newton gradient descent algorithm for searching the optimal solution is stated as follows:

$$\mathbf{b}_{k+1} = \mathbf{b}_k + \alpha_k \mathbf{d}_k,$$

$$\mathbf{d}_k = -\mathbf{D}_k \nabla L(\mathbf{b}_k), \tag{24}$$

where $\mathbf{D}_k$ is a positive definite matrix. The step size α_k is determined by a line search method. The line search method attempts to decrease the objective function along the curve defined by Eq. (24) by iteratively minimizing a polynomial approximation to the objective function. The quasi-Newton method possesses a fast rate of convergence while avoiding the Hessian matrix calculation associated with the original Newton method [20]. $\mathbf{D}_k$ is updated as follows:

$$\mathbf{D}_{k+1} = \mathbf{D}_k + \mathbf{D}_k^u, \tag{25}$$

where

$$\mathbf{D}_k^u = \frac{\mathbf{p}_k^{\mathrm{T}} \mathbf{p}_k}{\mathbf{p}_k^{\mathrm{T}} \mathbf{q}_k} - \frac{\mathbf{D}_k \mathbf{q}_k \mathbf{q}_k^{\mathrm{T}} \mathbf{D}_k}{\mathbf{q}_k^{\mathrm{T}} \mathbf{D}_k \mathbf{q}_k},$$

$$\mathbf{p}_k = \mathbf{b}_{k+1} - \mathbf{b}_k,$$

$$\mathbf{q}_k = \nabla L(\mathbf{b}_{k+1}) - \nabla L(\mathbf{b}_k). \tag{26}$$

This update scheme is used to approximate the Hessian matrix, and is also known as the Davidon–Fletcher–Powell method [20]. The complete algorithm is summarized as follows,

1. Input $\mathbf{b}_0$, $\mathbf{D}_0 = \mathbf{I}$, and termination criteria as
$$|\mathbf{b}_{k+1} - \mathbf{b}_k| < \varepsilon_{\mathbf{b}} \quad \text{or } |W_a(\mathbf{b}_{k+1}) - W_a(\mathbf{b}_{k+1})| < \varepsilon_{W_a}, \tag{27}$$
where $\varepsilon_{\mathbf{b}} = 10^{-6}$ and $\varepsilon_{W_a} = 10^{-5}$.
2. At the kth step, set $\mathbf{d}_k = -\mathbf{D}_k \nabla L(\mathbf{b}_k)$.

3. Compute the step size α_k according to the line search method, and set $\mathbf{b}_{k+1} = \mathbf{b}_k + \alpha_k \mathbf{d}_k$.
4. Compute the update matrix $\mathbf{D}_k^u$.
5. Set $\mathbf{D}_{k+1} = \mathbf{D}_k + \mathbf{D}_k^u$.
6. Continue with the $(k+1)$th step until the termination criteria are satisfied.

6. Numerical results

The optimization process is executed for three cases: tonal, narrowband and broadband. The same baseline beam is used in all cases. The baseline beam model introduced in Section 3.1 is employed with rectangular cells. The same weight and fundamental frequency constraints are applied to all cases. The total cell edge length of the baseline core is 6.2 m. The area of the baseline core where thickness of each edge is 0.01 m is $0.062\,m^2$, and the fundamental frequency is 81.8 Hz. The maximum core weight and the minimum fundamental frequency of the beam are determined by those of the baseline beam as $0.062\,m^2$ and 80 Hz, respectively. In tonal and narrowband examples, only the longitudinal movements of the cell nodes are considered as design parameters. The number of design parameters is 120. In the broadband example, the thicknesses of the core elements are added to the list of design parameters. The number of design parameters is increased to 258. To prevent crossing of adjacent nodes, a set of linear inequality constraints is also introduced by limiting nodal movements relative to the neighboring nodes. Also the movement of the right and left end nodes are fixed with a set of linear equality constraints.

6.1. Tonal optimization

For this case, we choose an excitation fixed at 700 Hz, which is off resonance for the baseline beam. From Fig. 7 the spectral distribution of the radiated acoustic power from the optimal beam to the one from the baseline beam can be compared. The reduction of the radiated power at the target frequency is marked in the graph and is approximately 22.1 dB. The attenuation of sound radiation at the target frequency can cause intensification of acoustic power at other frequencies, which is common with tonal optimizations. The optimal topology of the core is given in Fig. 8. The area of the optimal core is at the upper bound of the constraint $0.062\,m^2$. We also examine the sensitivity of the objective in optimal configuration as compared with the baseline one. In Fig. 9, the low level and uniform sensitivity distribution of the radiated acoustic power from the optimized beam relative to that of the baseline beam is shown. This indicates that the optimization has converged a local extremum.

The robustness of the tonal optimum is studied in a $\pm 10\%$ neighborhood of the optimized design parameters. Fig. 10 shows the variation of the radiated acoustic power in terms of the norm of perturbations

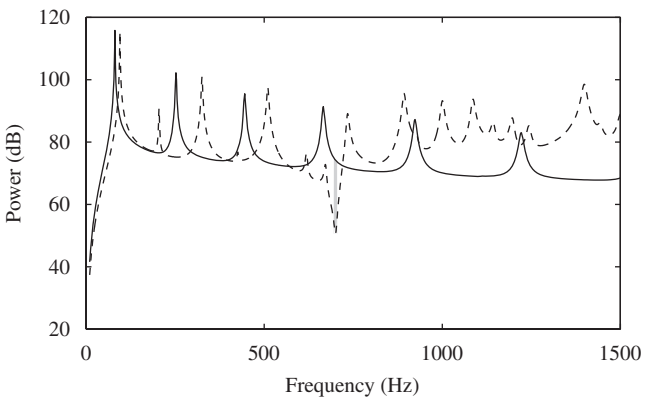

Fig. 7. Spectral distribution of the radiated sound power of the sandwich beam for tonal optimization. Dashed and solid lines, respectively, refer to the optimized and square cellular core baseline sandwich beams.

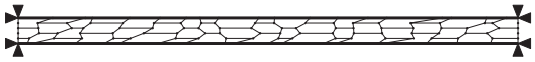

Fig. 8. Optimal core topology of the tonal case at 700 Hz.

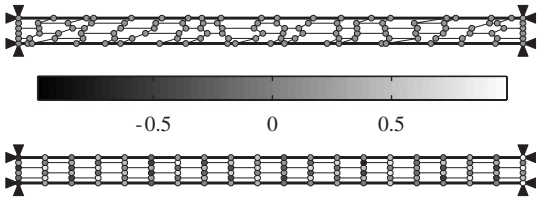

Fig. 9. The sensitivity of the power with respect to the longitudinal displacement of the nodes. The top plot is for the tonally optimized beam and the bottom one is for the baseline sandwich beam. Each circle shading level depicts the relative sensitivity which is normalized by its maximum amplitude.

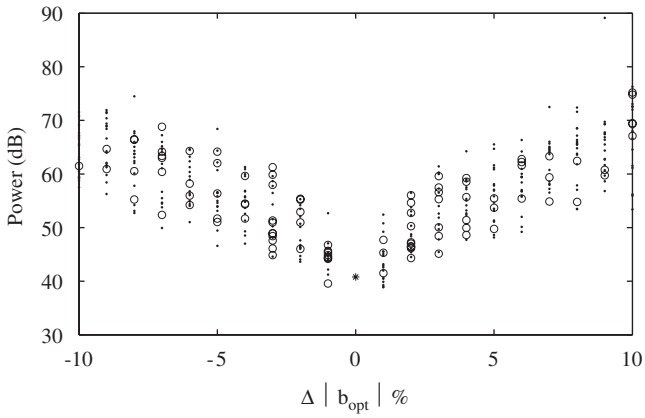

Fig. 10. Robustness of the tonal optimum in ±10% neighborhood of the optimized design parameters. The optimized power is denoted by a star marker at zero. The dots denote the power obtained by using the design parameters that violate the weight and fundamental frequency constraints. The circles denote the cases satisfying all the constraints.

of the design vector around the optimal one. Some randomly perturbed design parameters violate weight or fundamental frequency constraints or both. It is also noticeable from Fig. 10 that the randomly perturbed design parameters within the range of ±1% norm of perturbations from the optimal design parameters yield the acoustic power with a difference up to 15 dB as compared with the optimal response. This robustness with respect to the perturbations is important to manufacturing the optimal structures where variabilities are unavoidable.

Since the optimization problem contains a large number of design parameters and is nonlinear with respect to them, the search algorithm of optimization can reach only a local minimum starting from any initial condition. It is computationally intensive to study the effects of random initial configurations of the cellular core on the results of optimization. An example that uses the honeycomb cellular core as the initial and baseline beam is shown in Fig. 11. The frequency distributions of the radiated acoustic power from the baseline honeycomb beam and the optimized beam are presented in the figure. The optimization leads to a 20.0 dB reduction at 700 Hz. This is to be compared with the results in Fig. 7 where the square cellular core forms the baseline beam. The optimization with honeycomb baseline yields a different optimum than the one obtained by starting from the square core beam.

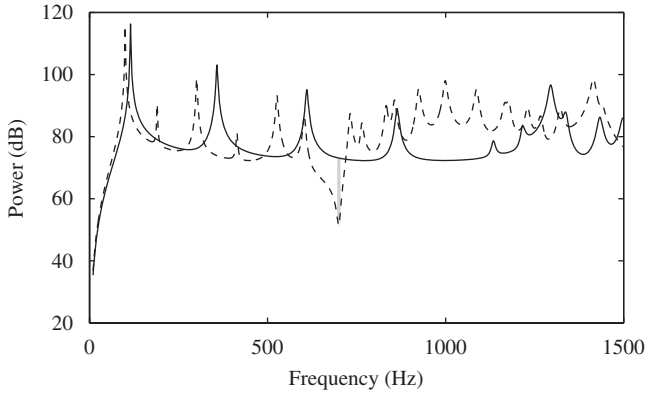

Fig. 11. Spectral distribution of the radiated sound power of the sandwich beam for tonal optimization. Dashed and solid lines, respectively, refer to the optimized and honeycomb core baseline sandwich beams.

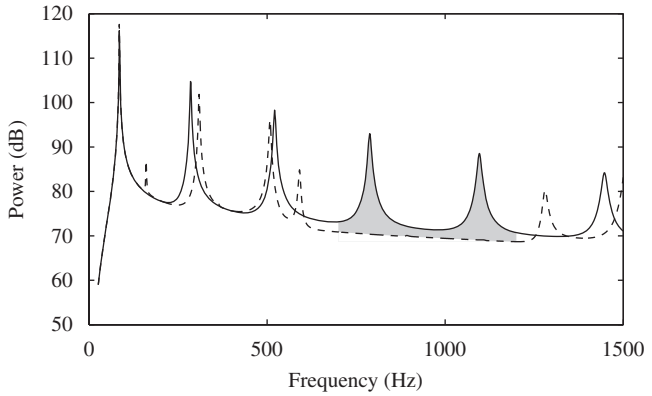

Fig. 12. Spectral distribution of the radiated sound power for the beam with narrowband optimization. Dashed and solid lines refer, respectively, to the optimized and the baseline sandwich beams. The shaded area depicts the reduction of the power over the targeted frequency band.

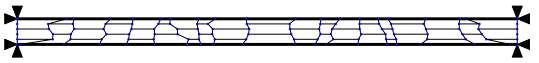

Fig. 13. Optimal core topology for the narrowband case.

6.2. Narrowband optimization

The frequency averaged power and its sensitivity are computed over a narrowband from 700 to 1200 Hz. The spectral variation of the power for the optimal and baseline beams are shown in Fig. 12. The reduction is highlighted by the gray area where frequency averaged reduction is around 5.2 dB. The optimal core is depicted in Fig. 13, and the sensitivity of the radiated acoustic power is shown in Fig. 14 for the baseline and optimized beams.

6.3. Broadband optimization

The targeted frequency band covers the range from 100 to 1000 Hz. The thickness of the cell frames are considered as design parameters in addition to the longitudinal movements of the nodes. Each node movement is bounded between −10 and 10 cm, and each frame thickness is limited between 0.1 and 5 cm. An optimal configuration of the core and frame thickness is obtained as shown in Fig. 15. The shading of the frames

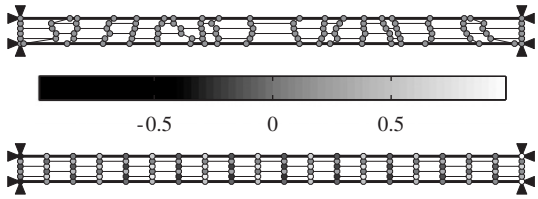

Fig. 14. The sensitivity of the power with respect to the longitudinal displacement of the nodes. The top plot is for the optimized sandwich beam for the narrowband case and the bottom one is for the baseline sandwich beam. Each circle shading level depicts the relative sensitivity which is normalized by its maximum amplitude.

Fig. 15. Optimal core topology for the broadband case. The frame shading level code of the core from white to black describes the thickness variation from 0.32 to 4.41 cm.

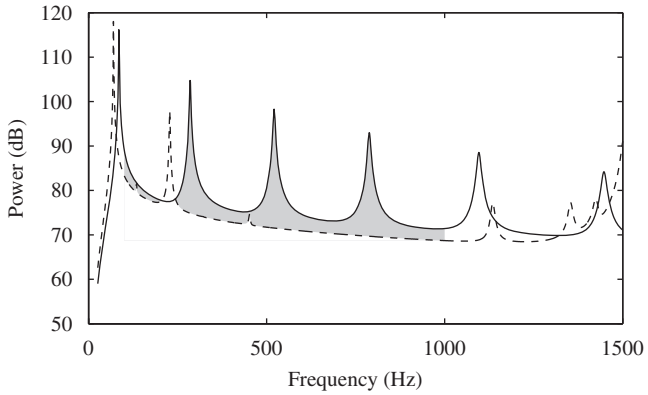

Fig. 16. Spectral distribution of the radiated sound power for the beam with broadband optimization. Dashed and solid lines refer, respectively, to the optimized and the baseline sandwich beams. The shaded area depicts the reduction of the power over the targeted frequency band.

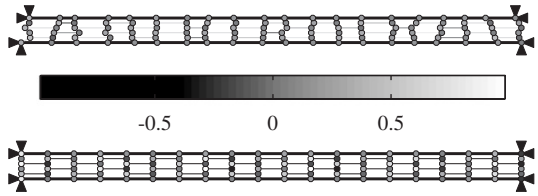

Fig. 17. The sensitivity of the power with respect to the longitudinal displacement of the nodes. The top plot is for the optimized sandwich beam in the broadband case and bottom one is for the baseline sandwich beam. Each circle shading level depicts the relative sensitivity which is normalized by its maximum amplitude.

indicates the thickness of the frame ranging from 0.32 to 4.41 cm. The radiated acoustic power variation of the beams in the frequency domain is given in Fig. 16. The average sound power reduction, represented by the gray area over the frequency band in the figure, is 4.9 dB. A sensitivity comparison of the optimized and baseline beams indicates that the optimized beam is less sensitive to the nodal movements than the baseline beam is as shown in Fig. 17.

The present optimization study does not consider manufacturability of the optimized structure. The design variables can also include the thickness and material properties of the cell in addition to the topology, making the optimized structure amenable to manufacturing. We have only allowed the nodes to move in the

longitudinal direction in the optimization study. The transverse movement of the nodes can also be considered. In general, more design parameters can lead to higher reduction of the radiated acoustic power.

7. Concluding remarks

We have presented an optimization study of the cellular core of sandwich structures to minimize the radiated sound power in a given frequency band, subject to constraints on the fundamental frequency and weight. Sensitivity functions are used in the optimization leading to more efficient and accurate numerical solutions. Numerical results for frequency, narrowband and broadband optimizations are presented. The longitudinal movements of core nodes and frame thicknesses are considered as design parameters in various cases. Other design parameters can also be considered in the optimization study including transverse movements of the nodes or material properties. The examples demonstrate that significant reduction of sound radiation can be achieved with the optimized core topology as compared with the baseline structure.

Acknowledgments

This research is supported by a Grant (CMS-0219217) from the National Science Foundation.

References

[1] J.R. Vinson, *The Behavior of Sandwich Structures and Isotropic Composite Materials*, Technomic Publishing Company, Lanchaster, Pennsylvania, 1999.
[2] J.R. Vinson, R.L. Sierakowski, *The Behavior of Structures of Composite Materials*, Kluwer Academic Publishers, Dordrecht, The Netherlands, 2002.
[3] M. Tinnsten, Optimization of acoustic response—a numerical and experimental comparison, *Structural and Multidisciplinary Optimization* 19 (2) (2000) 122–129.
[4] P. Thamburaj, J.Q. Sun, Optimization of anisotropic sandwich beams for higher sound transmission loss, *Journal of Sound and Vibration* 254 (1) (2002) 23–36.
[5] H. Denli, J.Q. Sun, T.W. Chou, Minimization of acoustic radiation from composite sandwich beam structures, *AIAA Journal* 43 (11) (2005) 2337–2341.
[6] A.G. Evans, J.W. Hutchinson, N.A. Fleck, M.F. Ashby, H.N.G. Wadley, Topological design of multifunctional cellular metals, *Progress in Materials Science* 46 (3–4) (2001) 309–327.
[7] M. Ruzzene, Vibration and sound radiation of sandwich beams with honeycomb truss core, *Journal of Sound and Vibration* 277 (4–5) (2004) 741–763.
[8] F. Scarpa, G. Tomlinson, Theoretical characteristics of the vibration of sandwich plates with in-plane negative Poisson's ratio values, *Journal of Sound and Vibration* 230 (1) (2000) 45–67.
[9] M. Ruzzene, F. Scarpa, F. Soranna, Wave beaming effects in two-dimensional cellular structures, *Smart Materials and Structures* 12 (3) (2003) 363–372.
[10] A.J. Keane, Passive vibration control via unusual geometries: the application of genetic algorithm optimization to structural design, *Journal of Sound and Vibration* 185 (3) (1995) 441–453.
[11] D.K. Anthony, S.J. Elliott, A.J. Keane, Robustness of optimal design solutions to reduce vibration transmission in a lightweight 2-D structure, part i: geometric design, *Journal of Sound and Vibration* 229 (3) (2000) 505–528.
[12] H. Denli, S. Frangakis, J.Q. Sun, Normalizations in acoustic optimization with Rayleigh integral, *Journal of Sound and Vibration* 284 (3–5) (2005) 1229–1238.
[13] G.H. Koopmann, J.B. Fahnline, *Designing Quiet Structures*, Academic Press, Inc., San Diego, CA, 1997.
[14] N. Wicks, J.W. Hutchinson, Optimal truss plates, *International Journal of Solids and Structures* 38 (30–31) (2001) 5165–5183.
[15] D. Prall, R.S. Lakes, Properties of a chiral honeycomb with a Poisson's ratio of −1, *International Journal of Mechanical Sciences* 39 (3) (1997) 305–314.
[16] K. Naghshineh, G.H. Koopmann, A.D. Belegundu, Material tailoring of structures to achieve a minimum radiation condition, *Journal of the Acoustical Society of America* 92 (2, Part 1) (1992) 841–855.
[17] R.R. Salagame, A.D. Belegundu, G.H. Koopmann, Analytical sensitivity of acoustic power radiated from plates, *Journal of Vibration and Acoustics* 117 (1) (1995) 43–48.
[18] N.H. Kim, J. Dong, K.K. Choi, N. Vlahopoulos, Z.D. Ma, M.P. Castanier, C. Pierre, Design sensitivity analysis for sequential structural-acoustic problems, *Journal of Sound and Vibration* 263 (3) (2003) 569–591.
[19] K.K. Choi, N.H. Kim, *Structural Sensitivity Analysis and Optimization*, Springer, Berlin, Germany, 2005.
[20] D.P. Bertsekas, *Constrained Optimization and Lagrange Multiplier Methods*, Academic Press, New York, 1982.